iScience

Article

Pathogenic *KIAA0586/TALPID3* variants are associated with defects in primary and motile cilia

Graphical abstract

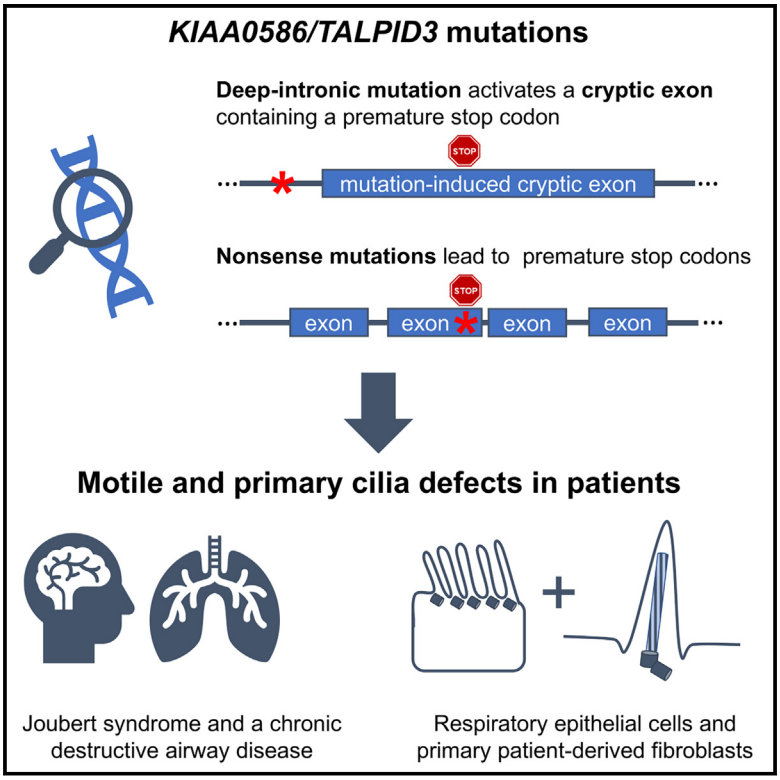

Highlights

- *KIAA0586/TALPID3* variants lead to Joubert syndrome including respiratory impairments
- Variants in *KIAA0586/TALPID3* affect both primary and motile cilia
- Deep-intronic sequence variant in *KIAA0586/TALPID3* activates a cryptic exon

Authors

Jacqueline E. Taudien, Diana Bracht, Heike Olbrich, ..., G. Christoph Korenke, Heymut Omran, John Neidhardt

Correspondence

john.neidhardt@uni-oldenburg.de

In brief

Cell biology; Cellular physiology; Human Genetics; Integrative aspects of cell biology

Taudien et al., 2025, iScience *28*, 111670
February 21, 2025
https://doi.org/10.1016/j.isci.2024.111670

CellPress

iScience

CellPress
OPEN ACCESS

Article

Pathogenic *KIAA0586/TALPID3* variants are associated with defects in primary and motile cilia

Jacqueline E. Taudien,[1,15] Diana Bracht,[2,15] Heike Olbrich,[2] Sebastian Swirski,[1,14] Fulvio D'Abrusco,[3] Bert Van der Zwaag,[4] Maike Möller,[1,13] Thomas Lücke,[5] Norbert Teig,[6] Ulrika Lindberg,[7] Kai Wohlgemuth,[2] Julia Wallmeier,[2] Anja Blanque,[8] Christos Gatsogiannis,[8] Sebastian George,[2] Christoph Jüschke,[1] Marta Owczarek-Lipska,[1,9] Dorothee Veer,[10] Hester Y. Kroes,[4] Enza Maria Valente,[3,11] G. Christoph Korenke,[12] Heymut Omran,[2,15] and John Neidhardt[1,9,15,16,*]

[1]Human Genetics, School of Medicine and Health Sciences, Carl von Ossietzky Universität Oldenburg, 26129 Oldenburg, Germany
[2]Department of General Paediatrics, University Hospital Muenster, 48149 Muenster, Germany
[3]Neurogenetics Research Centre, IRCCS Mondino Foundation, 27100 Pavia, Italy
[4]Division Laboratories, Pharmacy and Biomedical Genetics, Department of Genetics, University Medical Center of Utrecht, 3584 CX Utrecht, the Netherlands
[5]Department of Neuropaediatrics and Social Paediatrics, University Children's Hospital, Ruhr-University Bochum, 44791 Bochum, Germany
[6]Department of Neonatalogy, University Children's Hospital, Ruhr-University Bochum, 44791 Bochum, Germany
[7]Lund University, Skåne University Hospital, Department of Clinical Sciences Lund, Respiratory Medicine and Allergology, Lund, Sweden
[8]Institute for Medical Physics and Biophysics and Center for Soft Nanoscience (SoN), Westfälische Wilhelms University Münster, 48149 Münster, Germany
[9]Research Center Neurosensory Science, University of Oldenburg, 26129 Oldenburg, Germany
[10]Social-pediatric Outpatient and Therapy Center, Hospital Ludmillenstift, 49716 Meppen, Germany
[11]Department of Molecular Medicine, University of Pavia, 27100 Pavia, Italy
[12]University Children's Hospital Oldenburg, Department of Neuropaediatric and Metabolic Diseases, 26133 Oldenburg, Germany
[13]Present address: Division of Biochemistry, Department of Neuroscience, University of Oldenburg, 26129 Oldenburg, Germany
[14]Present address: Research Data Service Group, Leibniz Center for Tropical Marine Research, 28359 Bremen, Germany
[15]These authors contributed equally
[16]Lead contact
*Correspondence: john.neidhardt@uni-oldenburg.de
https://doi.org/10.1016/j.isci.2024.111670

SUMMARY

Pathogenic variants in *KIAA0586/TALPID3* are associated with the ciliopathy Joubert syndrome (JS). We report individuals with *KIAA0586/TALPID3* variants affected by primary and motile cilia defects leading to JS and chronic destructive airway disease. DNA variants were detected in three families by sequencing. In two unrelated families, a deep-intronic variant (*KIAA0586/TALPID3*:c.3990 + 3186G>A) activated a cryptic exon. We performed histological and functional analyses in native and air-liquid interface (ALI) cultured respiratory cells. Primary cilia lengths were measured in patient-derived fibroblasts. Our data associate *KIAA0586/TALPID3* variants with a syndrome combining JS and chronic destructive airway disease, reduced number of motile cilia, disorganized basal body location, and ciliary clearance malfunction. Additionally, patient-derived cell lines showed primary cilia defects. Disease causing *KIAA0586/TALPID3* variants, including a deep-intronic sequence variant, were associated with primary and motile cilia defects in JS patients. The combination of JS and respiratory symptoms should be considered indicative for *KIAA0586/TALPID3* sequence alterations.

INTRODUCTION

Joubert syndrome (JS, OMIM #616490) is a rare genetic and developmental disorder often diagnosed by a developmental defect of the cerebellum and the brainstem, the so called "molar tooth sign" (MTS), detectable by cerebral magnetic resonance imaging (MRI).[1] Genetic heterogeneity in JS-associated genes and a broad range of clinical phenotypic findings (e.g., apnea, ataxia, coloboma, developmental disorder, epilepsy, MTS and other brain anomalies, oculomotor apraxia, polydactyly, and tachypnea) complicates the diagnosis and treatment.[2–5]

JS-associated variants are nearly always inherited in an autosomal recessive fashion. The JS gene products are relevant for ciliogenesis and function of primary cilia, elongated cellular protrusions present on the surface of almost every cell of the human body. Primary cilia nucleate from basal bodies and contain a

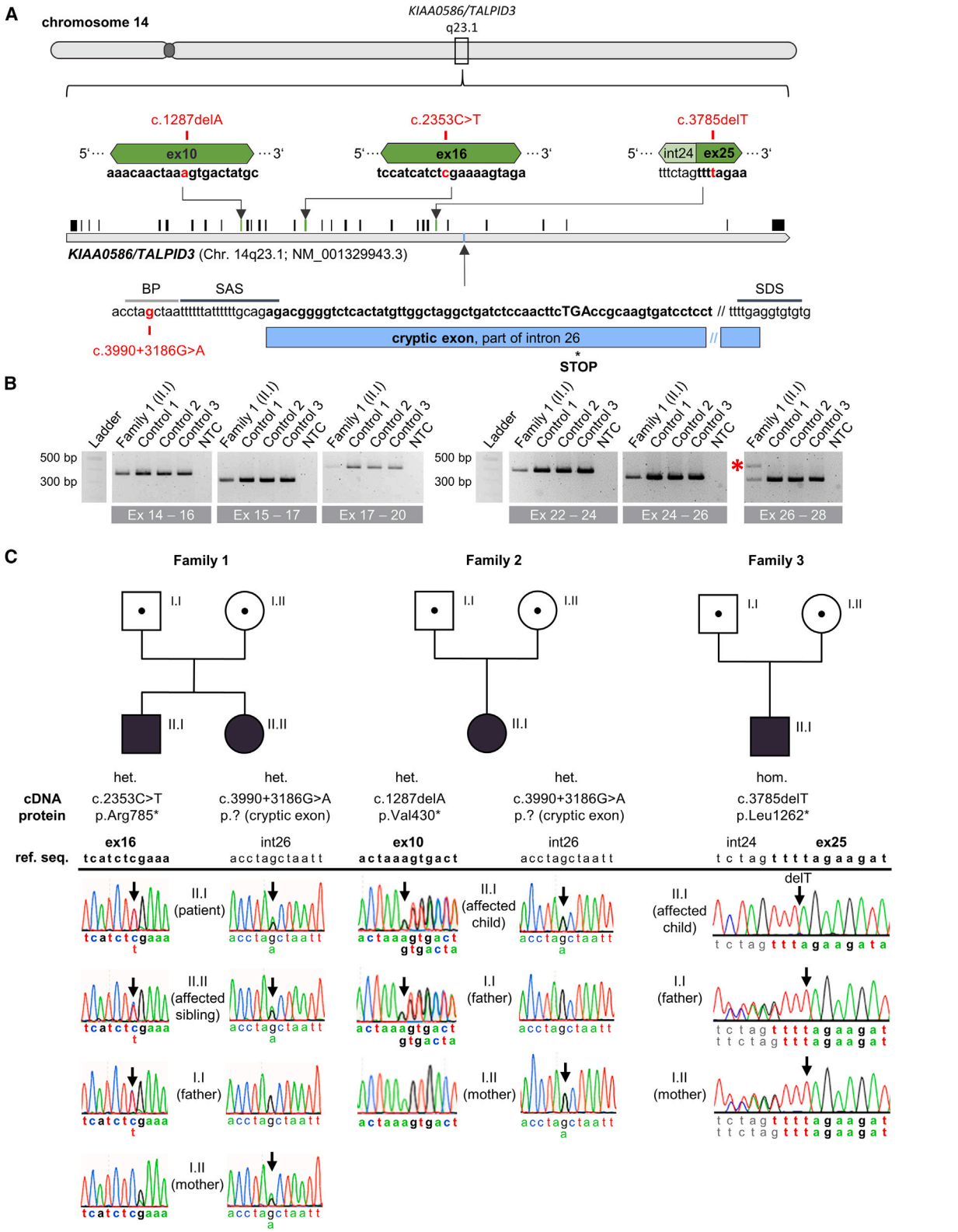

(legend on next page)

microtubule-based axoneme,[6,7] structures that regulate multiple signaling processes in proliferation and development.[8–10] Similar structural elements are also found in motile cilia. Nevertheless, JS has not been clearly associated with motile cilia dysfunction in the lung of human patients.[11] Motile cilia are present as a single rotating monocilium or as multiple bundles to disturb fluids or generate fluid flows. Multiciliated epithelial cells cover the upper and lower airways.[12–14] Impairment of the generation and differentiation of the respiratory epithelium can result in reduced numbers of multiple motile cilia, defective airway clearance function, and motile ciliopathy symptoms of chronic wet cough, rhinosinusitis, otitis media, recurrent pneumonia and/or bronchiectasis and atelectasis.[12–15]

KIAA0586/TALPID3 plays an important role in centrosomal migration and primary cilia formation and function.[16–18] Biallelic pathogenic variants in *KIAA0586/TALPID3* were associated with JS phenotypes.[19] While isolated respiratory symptoms have been reported for *KIAA0586/TAPLID3*-affected patients,[20] in this study we describe an overlapping syndrome, combining both primary and motile ciliopathies in human.

RESULTS

Pathogenic *KIAA0586/TALPID3* variants include deep-intronic sequence alterations

Clinical symptoms of four patients from three unrelated families not only included classical JS symptoms, but also severe chronic destructive airway disease. Based on the phenotypic similarities, we hypothesized to identify similar disease-associated sequence alterations in the genome of these patients. Indeed, our analyses revealed biallelic variants in *KIAA0586/TALPID3* in all affected patients, three of which carried an unknown type of *KIAA0586/TALPID3* variant located deep in intron 28 (Figure 1).

In the family 1, routine panel diagnostics revealed a heterozygous variant in *KIAA0586/TALPID3*:c.[2353C>T],[=]; p.Arg785* (NM_001329943.3) (Figure 1), which was verified in the index patient, his affected sister and the father using Sanger sequencing. The sequence alteration c.2353C>T; p.Arg785* was previously described as a likely-pathogenic variant.[21] Indications for copy number variations on the second allele were not identified. At this point of the analyses a second variant in *KIAA0586/TALPID3* was missing.

In the family 2, whole exome sequencing (WES) analysis of the index patient revealed only a single heterozygous likely-pathogenic variant *KIAA0586/TALPID3*:c.[1287delA],[=]; p.Val430* (NM_001329943.3) (Figure 1). The father was a carrier of this variant. Again, a second variant in *KIAA0586/TALPID3* was missing.

Consequently, gene diagnostic analyses in the family 1 and the family 2 did not explain the JS phenotype in the affected children, only revealing a single heterozygous nonsense variant in the *KIAA0586/TALPID3* gene. We therefore hypothesized that the missing variant on the second allele occurred in a deep-intronic region of the *KIAA0586/TALPID3* gene. As deep-intronic variants may interfere with proper splicing of the effected gene transcript, we used a fibroblast cell line derived from the index patient (II.I) of the family 1 and performed RT-PCR analyses. Comparing the *KIAA0586/TALPID3* transcript between patient-derived cells and healthy unrelated controls revealed an additional splice product with an increased fragment size generated between exons 26 and 28. This larger splice product was only detectable in the patient (Figure 1B, right) and indicated that a cryptic exon was included into the transcript, likely derived from intron 26 or 27. The additional splice product was sequenced and revealed 132 base pairs originating from deep-intronic parts of intron 26 in the *KIAA0586/TALPID3* gene. Targeted sequencing of the genomic region flanking the cryptic exon revealed the following deep-intronic variant in the index patient: *KIAA0586/TALPID3*:c.[3990 + 3186G>A],[=] (NM_001329943.3) (Figure 1). The variant is designated as rs571973649 and has been documented in GnomAD in 26 cases in a heterozygous state (SNV; 14-58495461-G-A (GRCh38)). The 26 cases primarily originated from Europe (non-Finnish) and the allele frequency was 0.0001712. The variant was not described in a homozygous state. So far, there are no reported clinical significances associated with this variant.

We found, that this deep-intronic base change from guanine to adenine generates the 5-mer motif CTRAY, which resembles highly conserved branchpoint (BP) sequences in humans.[22] The bioinformatic analysis programs ESEFinder 3.0 (http://krainer01.cshl.edu/cgi-bin/tools/ESE3/esefinder.cgi?process=home) calculated an increase in the BP score from 0.17 (without the variant) to 5.36 (with the variant). This finding was confirmed by applying SVM-BPfinder (http://regulatorygenomics.upf.edu/Software/SVM_BP/).

The deep-intronic sequence variant *KIAA0586/TALPID3:* c.[3990 + 3186G>A]; [=] (NM_001329943.3) activated a cryptic exon encoding 14 KIAA0586/TALPID3-unrelated amino acids followed by a premature termination codon at position 15 within the cryptic exon. The deep-intronic variant was detected in both JS-affected children of the family 1 and was inherited from the

Figure 1. Segregation analyses of *KIAA0586/TALPID3*-affected families

(A) Illustration of genetic variants identified in *KIAA0586/TALPID3* (NM_001329943.3; Chr. 14q23.1; 58,427,385-58,551,297; GRCh38:CM000676.2). Below the chromosome diagram, the *KIAA0586/TALPID3* gene is shown as a schematic drawing (light gray bar). The black marking above *KIAA0586/TALPID3* represent unaltered exons, while exons with variants are highlighted in green. The blue marking shows the cryptic exon in intron 26. Variants are depicted in red.

(B) RT-PCR analyses comparing the patient-derived fibroblast cell line (family 1, index patient [II.I]) with control fibroblasts. The coding region of exon 14 through 20 and exon 22 through 28 were amplified. Induced by the deep-intronic variant *KIAA0586/TALPID3*:c.(3990 + 3186G>A), the cryptic exon was spliced into the transcript and detected as an additional fragment (marked by a red asterisk).

(C) Pedigrees and electropherograms of Sanger sequencing results of three families carrying likely-pathogenic *KIAA0586/TALPID3*-variants (NM_001329943.3). The following variants cosegregated within families: family 1 c.[2353C>T]; c.[3990 + 3186G>A], family 2 c.[1287delA]; c.[3990 + 3186G>A], and family 3 c.[3785delT]; c.[3785delT]. NTC, non-template control; ref. seq., reference sequence; int, intron; ex, exon; BP, branchpoint; SAS, splice acceptor site; SDS, splice donor site.

Table 1. Overview of *KIAA0586/TALPID3* variants identified in this study

	Family 1 (II.I and II.II) het.		Family 2 (II.I) het.		Family 3 (II.I) hom.
NM_001329943.3	c.2353C>T	c.3990 + 3186G>A	c.1287delA	c.3990 + 3186G>A	c.3785delT
	p.Arg785*	p.?	p.Val430*	p.?	p.Leu1262*
NM_001244189.2	c.2512C>T	c.4149 + 3186G>A	c.1446delA	c.4149 + 3186G>A	c.3944delT
	p.Arg838*	p.?	p.Val483*	p.?	p.Leu1315*
genomic location (GRCh38/hg38)	chr14:58,467,833	chr14:58,495,461	chr14:58,456,735	chr14:58,495,461	chr14:58,490,167
GnomAD	14-58467833-C-T pathogenic af: 1.80e-5	14-58495461-G-A SNV af: 1.71e-4	not found	14-58495461-G-A SNV af: 1.71e-4	not found
clinVar	VariationID: 418265 Accession: VCV000418265.12 pathogenic	not found	not found	not found	not found
HGMD (public)	CM1510289 Missense/nonsense JS	not found	not found	not found	not found

The nomenclature of the variants refers to the MANE (matched annotation from NCBI and EMBL-EBI)-representative transcript (NM_001329943.3) and, additionally, to the transcript frequently used in KIAA0586 citations (NM_001244189.2). af, allele frequency; het., heterozygous; hom., homozygous.

unaffected mother (Figure 1C). Together with the heterozygous stop variant on the second allele, the deep-intronic base change explained the disease in the patients from family 1.

Significantly, targeted Sanger sequencing of the deep-intronic region in the family 2 revealed the same variant *KIAA0586/TALPID3:*c.[3990 + 3186G>A]; [=] (NM_001329943.3) in the index and the mother (Figure 1C). The combination of the single base pair deletion on one allele with the deep-intronic alteration on the second allele explained the disease symptoms of the index patient from family 2. A skin biopsy to culture patient-derived fibroblasts of the affected child of the family 2 was not available to the study.

WES analysis for patients of family 1 and 2 did not identify any other potential candidate variants in genes associated with cilia, PCD (primary ciliary dyskinesia), or JS.

In summary, our genetic data (branch point leading to cryptic exon activation; sequence change detected in several individuals with the same disease) support that the deep-intronic variant can be considered likely-pathogenic.

Patient (II.I) of family 3 was also found to carry variants in *KIAA0586/TALPID3*. WES analysis revealed the homozygous nonsense variant *KIAA0586/TALPID3*:c.[3785delT]; p.Leu1262* (NM_001329943.3) (Figure 1). No other candidate variant was found. Sanger sequencing confirmed the variant in the patient and identified the parents as heterozygous carriers.

For summary of all *KIAA0586/TALPID3* variants identified in the three families described in this study see Table 1.

Detailed clinical findings of *KIAA0586/TALPID3*-affected individuals

All individuals carry biallelic pathogenic *KIAA0586/TALPID3* variants and were diagnosed with chronic destructive airway disease in combination with JS symptoms.

The index patient (II.I) of the family 1 was born to unrelated healthy parents. He presented with neonatal respiratory distress. The diagnosis of JS was confirmed by MRI showing the typical MTS with an abnormally deep interpeduncular fossa and elongated, thick superior cerebellar peduncles (Figure 2A). Additionally, the index patient was diagnosed with epilepsy, chronic disease of the airways and a central respiratory regulation disorder typical for JS. Nasal nitric oxide (nNO) production rate was 51 nL/min (Table S1). The second child (II.II) from the family 1 also presented with respiratory distress after birth and was diagnosed with developmental delay including a respiratory regulation disorder (Table S1). The suspicion of JS was confirmed also by MRI, which detected the characteristic MTS (Figure 2A). Since birth, she suffers from chronic respiratory problems with recurrent bronchitis and persistent segmental lung atelectasis/dystelectasis as documented by MRI of the lungs (Figure 2B). The nNO production rate was 13 nL/min. Thus, both individuals show typical symptoms (neonatal respiratory distress, chronic disease of the airways) and findings (low nNO production rates below 77 nL/min) consistent with a respiratory ciliopathy.[23]

The patient (II.I) of family 2 has previously been described as a case report with orofacialdigital-like (OFD-like) syndrome in combination with symptoms of a chronic respiratory disease without genetic diagnosis.[24] The affected girl was born to unrelated healthy parents. She was reported with polydactyly, high arched palate, tongue hamartomas and dysmorphic face (Table S1). MRI showed slightly enlarged ventricles[24] and re-evaluation of the MRI findings identified the typical MTS consistent with JS (Figure 2A). The patient also reported neonatal respiratory distress and suffers from severe respiratory symptoms with upper and lower airway infections since birth. Computed tomography (CT) scans revealed atelectasis with suspicion of pneumonia postpartum and bronchiectasis[24] (Figure 2B). Stenram *et al.* already performed nasal and bronchial biopsies to analyze cilia of the affected girl. Transmission electron microscopy (TEM) data indicated a multiciliogenesis defect because of sparse number of cilia and mis-localized basal bodies responsible for the respiratory ciliopathy.[24]

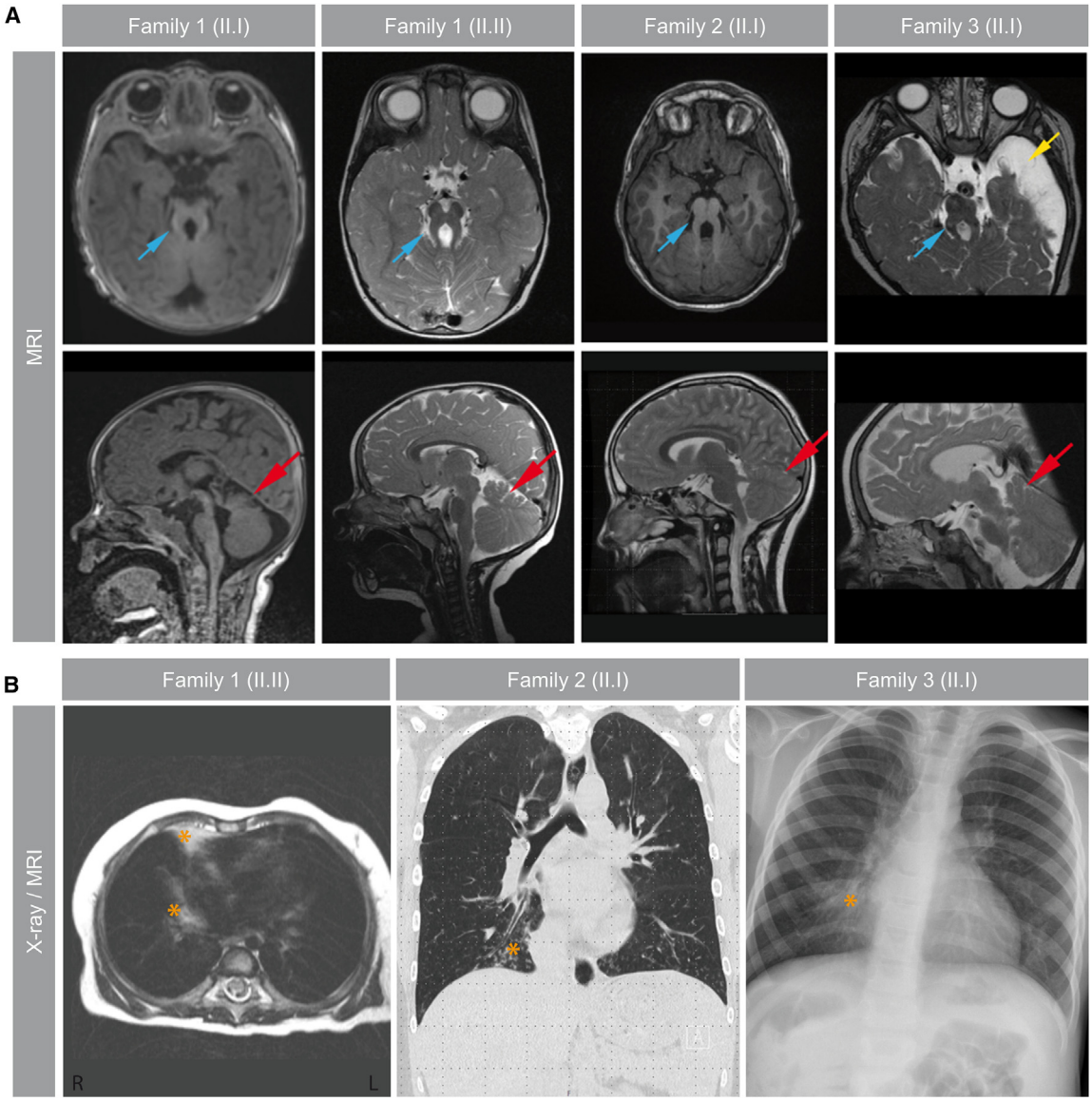

Figure 2. *KIAA0586/TALPID3*-affected individuals show JS-typical findings and destructive airway disease

(A) Cranial MRI of all affected individuals showed a molar tooth sign (MTS) (blue arrow). Transversal MRI panels show elongated superior cerebellar peduncles (blue arrow) as well as deepened interpeduncular fossa. Furthermore, patient (II.I) of family 3 additionally was affected by a left media infarct with secondary left-sided brain atrophy (yellow arrow). Midline saggital MRI panels illustrate dysplasia of the cerebellum (red arrow) (cerebellar vermis hypoplasia).

(B) MRI of the thorax of patient (II.II) of family 1 revealed middle and lower lobe dystelectasis (orange star). Chest CT of (II.I) of family 2 depicts bronchiectasis as well as mucous plugging (orange star). X-ray of the lungs of patient (II.I) of the family 3 documented chronic middle lobe dystelectasis (orange star).

The affected child (II.I) of the family 3 also presented with dysmorphic features such as polydactyly, neonatal respiratory distress and cerebral stroke (Table S1). MRI revealed cerebral arteria media infarction (left) with left sided atrophy (Figure 2A) and the MTS consistent with JS (Figure 2A). He also has a chronic disease of the airways since birth including chronic rhinosinusitis, chronic otitis media, chronic wet cough and bronchitis, recurrent pneumonia, chronic atelectasis of the middle lobe (Figure 2B) and repeatedly low nNO production rates (2 and 4 nL/min) also consistent with a respiratory ciliopathy.

Respiratory epithelial cells demonstrate defects in the generation of multiple motile cilia

Because we suspected in all affected patients a chronic respiratory ciliopathy, we analyzed patient-derived nasal multiciliated respiratory cells by TEM. For this purpose different material was used including native nasal respiratory cells directly after nasal brush biopsy and respiratory cells after cell culture.

The TEM analyses were carried out with differently handled nasal brush material of the *KIAA0586/TALPID3*-affected individuals: We used ALI-cultured cells from the first child (II.I) of family

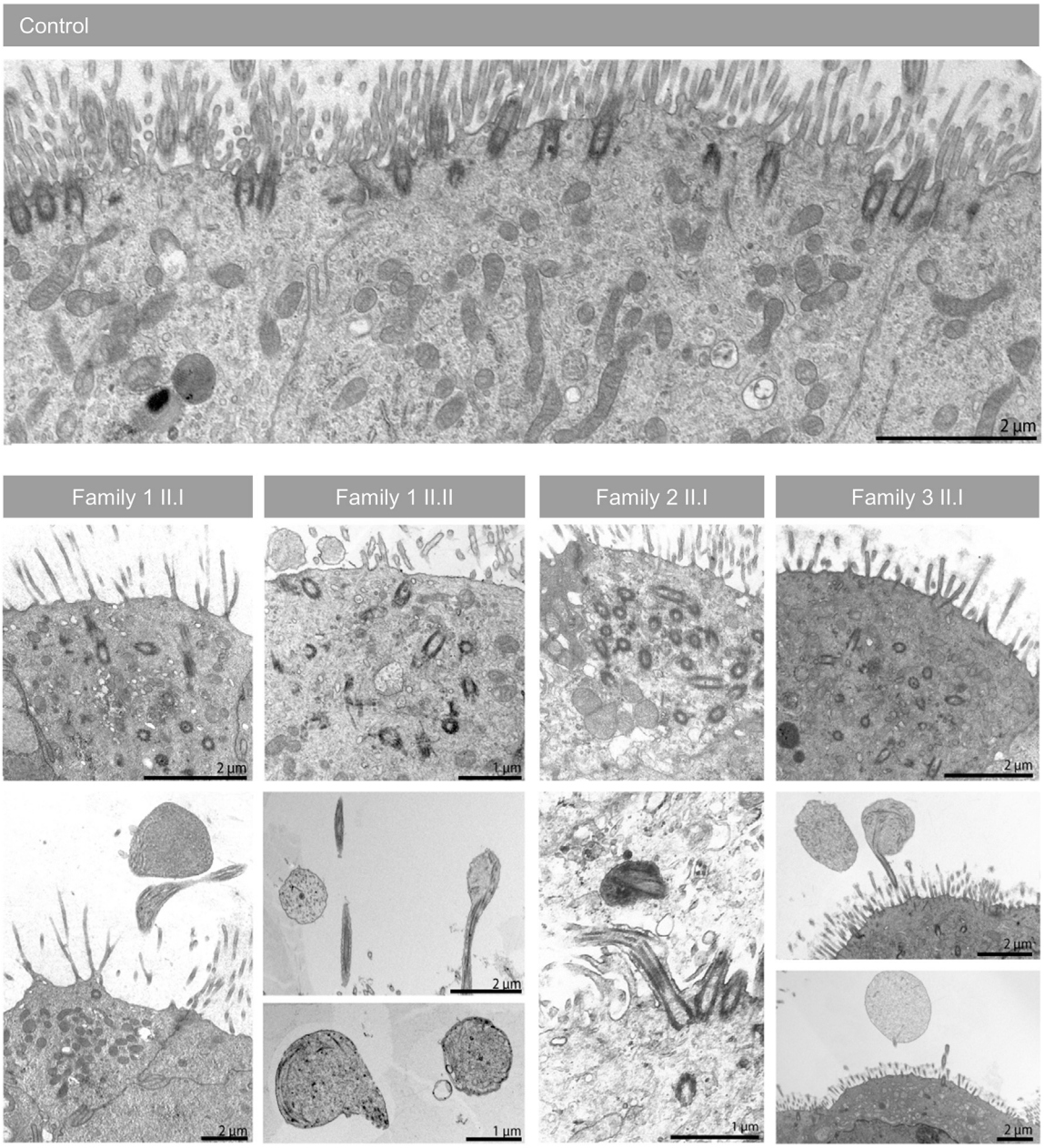

Figure 3. Transmission electron microscopy (TEM) of *KIAA0586/TALPID3*-affected respiratory epithelial cells revealed a defect in the generation of multiple motile cilia including reduced numbers of motile cilia, mis-localized basal bodies and bulbous ciliary tips in all four analyzed individuals

Respiratory epithelial cells were obtained by a nasal brush biopsy from a healthy control and affected individuals and subsequently analyzed by TEM (family 1 [II.I] TEM analyses after ALI; family 1 [II.II] and family 2 [II.I] TEM analysis directly after nasal brushing, family 3 [II.I] TEM analysis after spheroid cell culture). TEM pictures of the affected show a reduced number of multiple motile cilia, mis-localized basal bodies within the cytoplasm and cilia with bulbous tips. Scale bars represent as noted.

1, respiratory epithelial cells directly after brushing from the affected sibling (II.II; family 1) and also a spheroid cell culture of the affected child (II.I) of family 3. All TEM analyses revealed severely reduced numbers of cilia (Figure 3) for all patients. We also observed that the sparsely formed cilia showed structural abnormalities, like bulbous tips containing disorganized microtubules (Figure 3). Electron tomography illustrated this finding for (II.II) of family 1 (Figure S1). In addition, the number of basal bodies per cell appeared to be unaltered, but several of the basal bodies were mis-localized within the cytoplasm (Figures 3 and S2). Based on this finding, we re-analyzed the TEM data of patient (II.I) of family 2 in detail. Indeed, we were able to find the

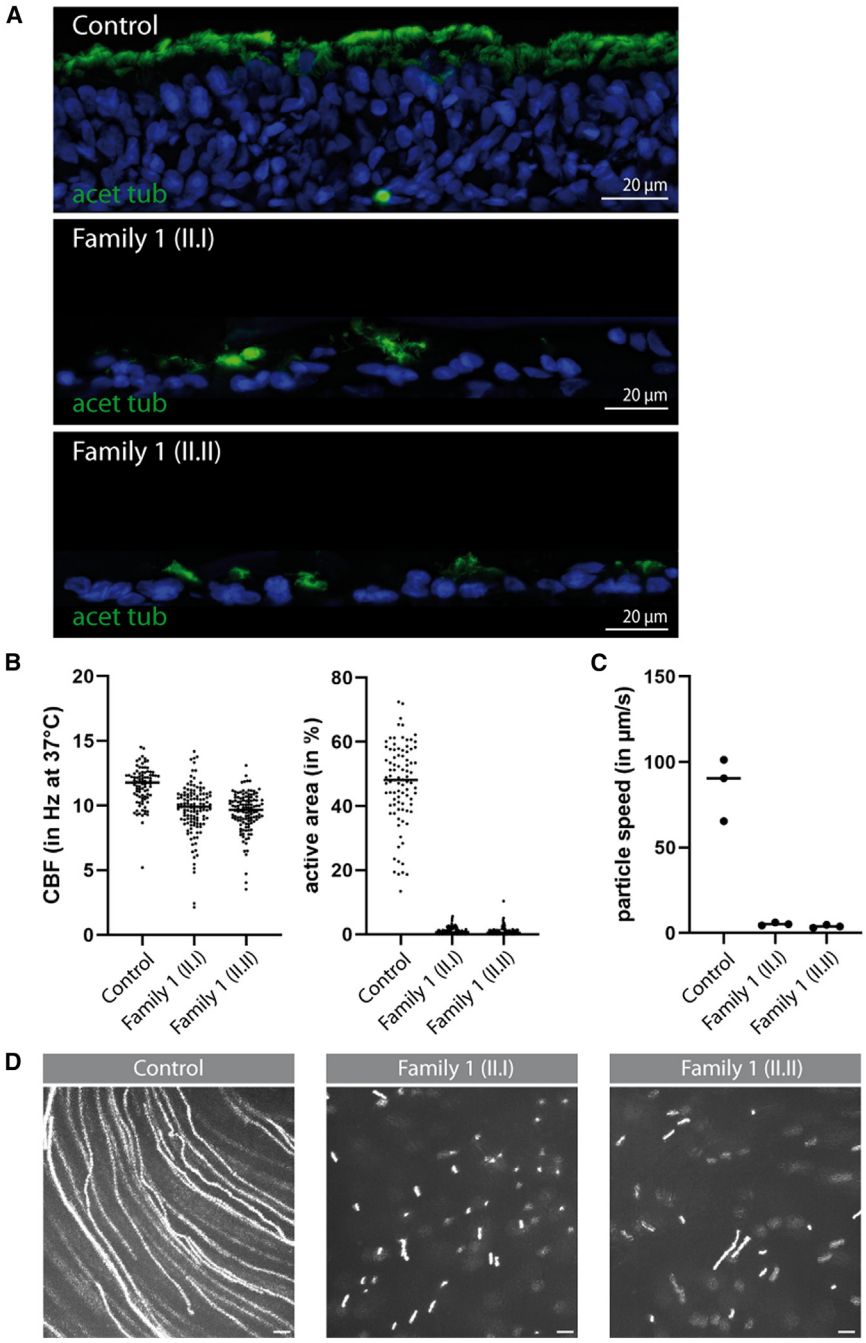

Figure 4. *KIAA0586/TALPID3*-affected respiratory epithelial cells cultured under ALI-conditions showed reduced number of beating cilia not sufficient to maintain mucociliary clearance *in vitro*

(A) After full differentiation, ALI-cultures were stained with antibodies directed against acetylated alpha-tubulin (acet tub; green) to mark the ciliary axoneme. Nuclei were stained with Hoechst (blue).

(B) Left graph: CBF was measured and within normal range for all tested individuals (control: 12 Hz ± 1 Hz; family 1 [II.I]: 11 Hz ± 7 Hz; family 1 [II.II]: 10 Hz ± 3 Hz). Right graph: the calculated active area reflecting ciliary beat movement was markedly reduced in ALI-cultures of the affected individuals (control: 47% ± 13%; family 1 [II.I]: 1% ± 1%; family 1 [II.II]: 1% ± 1%).

(C) Statistical analyses of three independent particle tracking experiments per individual revealed reduced speed of transported particles for *KIAA0586/TALPID3*-affected ALI-cultures (control: 86 µm/s; family 1 [II.I]: 5 µm/s; family 1 [II.II]: 4 µm/s).

(D) Particle tracking videos given as z stack projections are exemplary shown per individual. Scale bars in (D) represent 100 µm.

structural changes of the ciliary tip as well as the reported abnormalities of the basal bodies (Figures 3 and S2). In conclusion, variants in *KIAA0586/TALPID3* can lead to severe defects in the generation of multiple motile cilia including reduced numbers of motile cilia per cell, mis-localized basal bodies, and bulbous ciliary tips. These findings are consistent with a defect also referred to as reduced generation of multiple motile cilia (RGMC).[13]

Because some RGMC disorders also result in defects of the differentiation of the airway cells, we performed immunofluorescence (IF) stainings of cryo-sections of ALI-cultures. Multiciliated respiratory cells were analyzed using anti-acetylated alpha-tubulin antibody to label ciliary axonemes. Indeed, ALI-cultures derived from both patients of family 1 showed a reduced number of multiciliated cells. Bundles of axonemes were only occasionally detected (Figure 4). In addition, we noticed a reduced cell layer thickness in *KIAA0586/TALPID3*-deficient ALI-cultures (Figure 4A) indicating a defect in proliferation and differentiation of the respiratory epithelium.

Next, we asked whether the structural abnormalities identified in the *KIAA0586/TALPID3* patient-derived respiratory cells indeed result in abnormal ciliary beating. To answer this question we performed high-speed video micoscopy analyses (HSVM) of respiratory cells originating from ALI-cultures of a control and patients (II.I) and (II.II) of family 1 (Videos S1, S2, and S3; spheroid cells of a control and patient (II.I) of family 3: Videos S4 and S5). HSVM, revealed few and stiffly beating cilia (analyses of the ALI-cultures of patients [II.I] and [II.II] of family 1 showed that the average ciliary beat frequency [CBF] was within normal lower ranges) (Figure 4B). Next we asked whether the residual cilia of *KIAA0586/TALPID3* patient-derived cells are able to generate fluid flows along their surfaces in order to assess ciliary clearance capacity. Analyses of the ALI-cultures of the affected individuals showed reduced active areas in

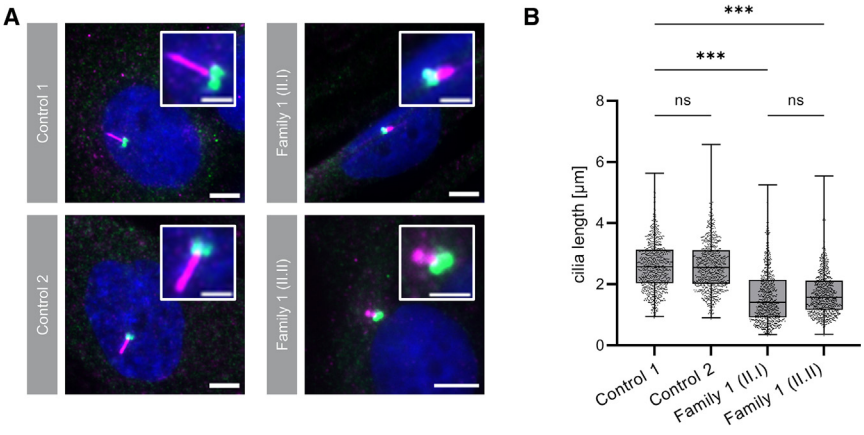

Figure 5. Primary cilia length measurement

(A) Images of primary cilia from patient-derived fibroblasts in comparison to two unrelated healthy controls. The axonemes are shown in magenta (detyrosinated tubulin), basal bodies in green (γ-tubulin). Primary cilia of the patient (II.I and II.II) of family 1 showed normal basal bodies and shortend axonemes.

(B) The length of primary cilia from patient-derived fibroblasts and from unrelated controls were quantified. In total 750 cilia per cell line were measured in three independent experiments (250 cilia per experiment). The median of the box blots showed 2.6 μm in controls and 1.4 μm and 1.5 μm in the patients. Statistical analysis was performed applying Kruskal-Wallis statistical test. Scale bars: 5 μm, 1 μm for inset; ***: p value < 0.0001; ns: not significant.

comparison to healthy control cultures (Figure 4B). This suggested an impaired ability to maintain ciliary clearance in *KIAA0586/TALPID3*-affected cells. Indeed, particle tracking experiments using fluorescent-labeled beads in *KIAA0586/TALPID3*-deficient ALI-cultures demonstrated that the affected respiratory epithelial cells were unable to propel fluid along their epithelia. In contrast, the healthy control showed a directed fluid movement (Figures 4C and 4D; Videos S6, S7, and S8). In summary, our findings demonstrate a defect in the generation of multiple motile cilia including reduced numbers of motile cilia, mislocalized basal bodies and bulbous ciliary tips in individuals with *KIAA0586/TALPID3* variants studied herein. The few residual cilia are unable to provide adequate ciliary clearance of the airway surface explaining the severe respiratory phenotype of the affected individuals.

Primary cilia length is reduced in patients with biallelic *KIAA0586/TALPID3* variants

JS was previously described as a defect of primary cilia, the type of cilia that is present on almost all cell types including neuronal cells. To verify whether the *KIAA0586/TALPID* variants lead to primary cilia defects, we analyzed patient-derived fibroblasts cell lines. We included cell lines derived from patient (II.I) and (II.II) (Figure 5) of family 1 that carried the novel deep-intronic variant *KIAA0586/TALPID3*:c.3990 + 3186G>A (NM_001329943.3) in combination with the nonsense mutation c.2353C>T. The patient-derived cell lines showed significantly shortened ciliary axonemes consistent with a defect in primary cilia formation and/or maintenance.

DISCUSSION

Patients with ciliary dysfunction often suffer from combinations of different symptoms. Well-described examples are the Bardet-Biedl syndrome and JS, which are predominantly associated with defects of the primary cilium,[3,25] frequently leading to renal disorders, retinopathies, skeletal malformations, and anomalies of the brain.[23,26,27] In contrast, phenotypes of PCD or RGMC are associated with defects in motile cilia.[12,13,23,28,29] Indeed, ciliopathies constitute a considerable burden to patients and families, and novel therapeutic approaches are urgently needed.

Herein, we report four patients from three unrelated families affected by pathogenic *KIAA0586/TALPID3* variants. Clinical diagnoses included JS-characteristic findings in addition to severe lung disease. Standard gene diagnostic testing did not identify the genetic cause of the clinical diagnoses, either due to an undetected deep-intronic variant, or due to the analysis of a limited gene panel focused on a subset of the syndromic features. Our data imply that patients with extended syndromic features will benefit from broad diagnostic analyses such as whole genome sequencing.

KIAA0586/TALPID3 is one of the known genes whose mutations can lead to JS.[4,28] Pathogenic variants in this gene previously were associated with severe defects of primary cilia.[16,30] KIAA0586/TALPID3 interacts with several ciliary proteins and localizes to the distal end of the centrioles.[21,31–38] Loss of functional KIAA0586/TALPID3 prevented the dissociation of centriolar proteins involved in distal appendage assembly, centriole maturation, and primary cilia formation.[32,34,38] In *kiaa0586/talpid3* animal models, defects of motile cilia were previously reported to lead to a failure of centrosomal migration in ependymal cells (chicken), loss of motile cilia in the floorplate of the neural tube (chicken) and length of motile cilia in Kupffer's vesicle (zebrafish).[17,30,39,40] This study associates pathogenic *KIAA0586/TALPID3* variants with motile cilia defects in the lung of human patients.

Here, we demonstrate that human motile respiratory cilia are also affected by *KIAA0586/TALPID3* variants. Failure of adequate ciliary airway clearance was found in *KIAA0586/TALPID3*-affected individuals and associated with chronic upper and lower airway infections. Recurrent middle ear infections, bronchiectasis, and atelectasis are typical phenotypes of motile ciliopathies.[13] Indeed, the reduced number of respiratory motile cilia fits into the RGMC-disease group rather than into the classical PCD disease group.[12–15,23] Unlike in *MCIDAS*- and *CCNO*-affected respiratory cells from RGMC patients, the number of basal bodies seemed to be normal but mis-localized within the cytoplasm in *KIAA0586/TALPID3*-affected multiciliated cells (Figures 3 and S2).[12,13] This is consistent with a defect in basal body transport to the subapical membranes as recently

reported by Stephen *et al.*,[30] rather than a defect in basal body amplification present in *MCIDAS* and *CCNO*-affected respiratory cells. Moreover, we analyzed the centrioles by IF staining with polyclonal anti-CEP164 antibodies (component of distal appendages) as reported for primary and motile cilia by Kobayashi *et al.*, Alby *et al.* and Stephen *et al.*[2,21,32] Consistent with the previous publications, CEP164 was detected in the control as well as the *KIAA0586/TALPID3*-affected multiciliated cells of patient (II.I) and (II.II) of family 1 indicating that the assembly of CEP164 to the basal bodies is not affected. However, CEP164 was also detected in the cytoplasm of the affected cells of (II.I) and (II.II), which is consistent with a defect in basal body migration (Figure S3). In addition to the defect in the generation of multiple motile cilia (Figure 3), we also observed a defect in proliferation and differentiation of airway cells (Figure 4A) similar to RGMC-affected individuals with *TP73* variants.[15] Nevertheless, we cannot exclude completely that the number of basal cells or cell culture conditions influenced the proliferation or differentiation of air-liquid interface (ALI) cultures. *In vitro*, we found less proliferated epithelia with a decreased number of multiciliated cells. Furthermore, the *KIAA0586/TALPID3*-affected motile cilia show bulbous tips with mis-orientated microtubules. Similar ciliary defects were described for gene defects in *TUBB4B*, in which a subset of sequence alterations was associated with only PCD.[41] Molecularly, KIAA0586/TALPID3 forms a ring like-structure at the distal end of centrioles and localizes in spatial proximity to the JS-associated OFD1.[34,42,43] Loss-of-function of *OFD1* on the X chromosome indeed is associated with defects in primary as well as motile cilia and leads to a combination of JS symptoms including chronic destructive airway disease in males.[43]

Current treatment strategies of motile ciliopathies are mostly symptomatic including a combination of inhalation, physiotherapy, and antibiotic treatment, focusing on the amelioration of the progression of the disease or to improve the quality of life of the patient. Genetic heterogeneity and clinical variability puts obstacles to targeted therapies.[23] Of note, the cryptic exon, which was generated by the deep-intronic variant, may be treatable with small RNAs, e.g., antisense oligonucleotides (AONs). AONs offer promising therapeutic approaches and have been successfully applied to restore aberrant splice defects in *ABCA4* and *CEP290*, two examples of autosomal recessively inherited genes with pathogenic deep-intronic variants.[44,45]

Ciliopathy-related deep-intronic variants were also identified in the genes *USH2A* and *OFD1*.[46,47] The interference of cryptic exons with splicing of transcripts only recently has been recognized to be a relevant factor in genetic diseases.[48–50] Deep-intronic regions were not yet described to carry pathogenic variants in the gene *KIAA0586/TALPID3*. Notably, additional JS patients were reported to carry only a single heterozygous pathogenic variant in *KIAA0586/TALPID3*.[19,51] Thus, it seems quite conceivable that such patients carry a deep-intronic variant on the second allele in *KIAA0586/TALPID3*.

Together, *KIAA0586/TALPID3* variants are associated with a combination of JS and chronic respiratory disease, likely caused by a dual function of the protein in both, primary and motile cilia. Deep-intronic variants in *KIAA0586/TALPID3* should be considered in the genetic diagnosis of patients and provide possible target sites toward the development of treatment approaches, e.g., applying small RNA-therapeutics.

Limitations of the study

We identified rare compound heterozygous variants in *KIAA0586/TALPID3* in four patients from three independent families affect by JS and chronic destructive airway disease. Additional patients/families and functional studies are needed to further strengthen and fully understand the nature of this overlapping syndrome. A higher number of patients is also desirable to accurately determine the percentage of patients suffering from both JS and respiratory disorders. It will be interesting to search for deep-intronic alterations influencing transcript processing of *KIAA0586/TALPID3* in so far unsolved cases with only a single heterozygous mutation detected in the coding region.

While our study provides important insights into the effects of *KIAA0586/TALPID3* mutations on primary and motile cilia in human, there are areas of cell biology that could be explored further. For example, it remains unclear whether the undocked centrioles in human patients show an altered length, as shown for animal models. Although we have gained significant findings relevant to the clinical implications for JS patients, a more in-depth exploration of centrosomal cell biology might open new opportunities to improve the understanding of the KIAA0586/Talpid3 function. Future studies might thus focus on the understanding of the cellular pathology associated with *KIAA0586/TALPID3* mutations.

RESOURCE AVAILABILITY

Lead contact

Further information and requests for resources and reagents should be directed to and will be fulfilled by the lead contact Prof. Dr. John Neidhardt (john.neidhardt@uni-oldenburg.de).

Materials availability

This study did not generate new unique reagents.

Data and code availability

- Access to data presented will be provided upon request. This study includes no data deposited in external repositories.
- This paper does not report original code.
- Additional information necessary to reanalyze the data or reinterpret the reported findings is available upon request.

ACKNOWLEDGMENTS

We are especially grateful for the willingness of patients and families to provide biological material and medical data for research. We thank Jannis Eilers, Dennis Kastrati, and Kerstin Stegmann from the Human Genetics at the University Oldenburg for technical assistance. Furthermore, we are grateful to Matina Herting, Andreas Borgscheiper, Sironi Sivalingam, Laura Schwiddessen, Hannah Schmidt, and Borami Shin from the Department of General Pediatrics at Muenster University Hospital for technical support. We specifically would like to acknowledge the contribution of Unne Stenram (Lund), who recently deceased and previously described ciliogenesis defects in respiratory cilia of family 2 using TEM.[24] The Department of General Pediatrics at the University Hospital Münster is full member of the European Reference Networks (ERN) for rare respiratory diseases (ERN-LUNG), rare kidney diseases (ERKNet) and rare malformation syndromes, intellectual and other neurodevelopmental disorders (ERN-ITHACA). Funding for this work was provided by: (1) The School

of Medicine and Health Sciences at the University Oldenburg (FP 2022-064), by the European Union E-Rare program (NE 2118/2-1), and the DFG Priority Programms (NE 2118/3-1) to J.N.; (2) Telethon Italy (GGP20070) and Italian Ministry of Health (RF-2019-12369368) to E.M.V.; (3) DFG OM6/10 and BMBF NEOCYST-(01GM1515A, 01GM1903A, 01GM2203A) to H. Omran; and (4) DFG (WA 4283/1-1) and Interdiziplinäres Zentrum für Klinische Forschung Muenster (IZKF SEED/017/21) to J.W.

AUTHOR CONTRIBUTIONS

Authors are listed in alphabetical order not by contribution. Study design: D.B., H. Omran, J.N., and J.E.T.; clinical characterization: G.C.K., D.V., H. Omran, J.N., J.W., N.T., T.L., and U.L.; genetic characterization: C.J., D.B., H. Olbrich, J.N., J.E.T., and M.O.-L.; data collection: A.B., C.G., C.J., D.B., H. Olbrich, J.E.T., M.O.-L., and S.S.; experimental assistance: K.W., and M.M.; data analyses: D.B., H. Omran, J.N., J.E.T., K.W., and S.G.; screening of patient cohorts: B.V.d.Z., E.M.V., F.D., H.Y.K., and H. Olbrich; draft manuscript writing: D.B., H. Omran, J.N., J.E.T., and J.W.; manuscript curation: D.B., H. Omran, J.N., and J.E.T.

G.C.K. is managing the clinical findings of family 1. J.N. manages family 1-related genetic and primary cilia material and data. H. Omran oversees the clinical findings, data, and materials of family 2 and 3 and motile cilia.

All authors reviewed and approved the final manuscript version.

DECLARATION OF INTERESTS

The authors declare no competing interests.

STAR★METHODS

Detailed methods are provided in the online version of this paper and include the following:

- KEY RESOURCES TABLE
- EXPERIMENTAL MODEL AND STUDY PARTICIPANT DETAILS
  - Ethics statement
  - Culture of respiratory epithelial cells
  - Culture of fibroblast cells
- METHOD DETAILS
  - DNA extraction and genetic analysis
  - PCR amplification and sanger sequencing
  - TEM and 3D tomography
  - IF staining of respiratory epithelial cells
  - High-speed video microscopy
  - Particle tracking experiments
  - RNA isolation and RT-PCR analyses
  - Immunocytochemistry of fibroblast cells
  - Measurements of primary cilia
- QUANTIFICATION AND STATISTICAL ANALYSIS

SUPPLEMENTAL INFORMATION

Supplemental information can be found online at https://doi.org/10.1016/j.isci.2024.111670.

Received: June 19, 2024
Revised: September 18, 2024
Accepted: December 19, 2024
Published: December 21, 2024

REFERENCES

1. Maria, B.L., Hoang, K.B., Tusa, R.J., Mancuso, A.A., Hamed, L.M., Quisling, R.G., Hove, M.T., Fennell, E.B., Booth-Jones, M., Ringdahl, D.M., et al. (1997). "Joubert syndrome" revisited: key ocular motor signs with magnetic resonance imaging correlation. J. Child Neurol. *12*, 423–430.
2. Alby, C., Piquand, K., Huber, C., Megarbané, A., Ichkou, A., Legendre, M., Pelluard, F., Encha-Ravazi, F., Abi-Tayeh, G., Bessières, B., et al. (2015). Mutations in KIAA0586 Cause Lethal Ciliopathies Ranging from a Hydrolethalus Phenotype to Short-Rib Polydactyly Syndrome. Am. J. Hum. Genet. *97*, 311–318.
3. Bachmann-Gagescu, R., Dempsey, J.C., Phelps, I.G., O'Roak, B.J., Knutzen, D.M., Rue, T.C., Ishak, G.E., Isabella, C.R., Gorden, N., Adkins, J., et al. (2015). Joubert syndrome: a model for untangling recessive disorders with extreme genetic heterogeneity. J. Med. Genet. *52*, 514–522.
4. Parisi, M., and Glass, I. (2003). Joubert Syndrome. In GeneReviews® [Internet], M.P. Adam, J. Feldman, G.M. Mirzaa, R.A. Pagon, S.E. Wallace, and A. Amemiya, eds. (Seattle: University of Washington), pp. 1993–2024. https://www.ncbi.nlm.nih.gov/books/NBK1325/.
5. Brancati, F., Dallapiccola, B., and Valente, E.M. (2010). Joubert Syndrome and related disorders. Orphanet J. Rare Dis. *5*, 20.
6. Carvalho-Santos, Z., Azimzadeh, J., Pereira-Leal, J.B., and Bettencourt-Dias, M. (2011). Evolution: Tracing the origins of centrioles, cilia, and flagella. J. Cell Biol. *194*, 165–175.
7. Fisch, C., and Dupuis-Williams, P. (2011). Ultrastructure of cilia and flagella - back to the future. Biol. Cell. *103*, 249–270.
8. Singla, V., and Reiter, J.F. (2006). The primary cilium as the cell's antenna: signaling at a sensory organelle. Science *313*, 629–633.
9. D'Angelo, A., and Franco, B. (2009). The dynamic cilium in human diseases. Pathogenetics *2*, 3.
10. Park, S.M., Jang, H.J., and Lee, J.H. (2019). Roles of Primary Cilia in the Developing Brain. Front. Cell. Neurosci. *13*, 218.
11. Parisi, M.A. (2019). The molecular genetics of Joubert syndrome and related ciliopathies: The challenges of genetic and phenotypic heterogeneity. Transl. Sci. Rare Dis. *4*, 25–49.
12. Boon, M., Wallmeier, J., Ma, L., Loges, N.T., Jaspers, M., Olbrich, H., Dougherty, G.W., Raidt, J., Werner, C., Amirav, I., et al. (2014). MCIDAS mutations result in a mucociliary clearance disorder with reduced generation of multiple motile cilia. Nat. Commun. *5*, 4418.
13. Wallmeier, J., Al-Mutairi, D.A., Chen, C.-T., Loges, N.T., Pennekamp, P., Menchen, T., Ma, L., Shamseldin, H.E., Olbrich, H., Dougherty, G.W., et al. (2014). Mutations in CCNO result in congenital mucociliary clearance disorder with reduced generation of multiple motile cilia. Nat. Genet. *46*, 646–651.
14. Wallmeier, J., Frank, D., Shoemark, A., Nöthe-Menchen, T., Cindric, S., Olbrich, H., Loges, N.T., Aprea, I., Dougherty, G.W., Pennekamp, P., et al. (2019). De Novo Mutations in FOXJ1 Result in a Motile Ciliopathy with Hydrocephalus and Randomization of Left/Right Body Asymmetry. Am. J. Hum. Genet. *105*, 1030–1039.
15. Wallmeier, J., Bracht, D., Alsaif, H.S., Dougherty, G.W., Olbrich, H., Cindric, S., Dzietko, M., Heyer, C., Teig, N., Thiels, C., et al. (2021). Mutations in TP73 cause impaired mucociliary clearance and lissencephaly. Am. J. Hum. Genet. *108*, 1318–1329.
16. Yin, Y., Bangs, F., Paton, I.R., Prescott, A., James, J., Davey, M.G., Whitley, P., Genikhovich, G., Technau, U., Burt, D.W., and Tickle, C. (2009). The Talpid3 gene (KIAA0586) encodes a centrosomal protein that is essential for primary cilia formation. Development *136*, 655–664.
17. Ben, J., Elworthy, S., Ng, A.S.M., van Eeden, F., and Ingham, P.W. (2011). Targeted mutation of the talpid3 gene in zebrafish reveals its conserved requirement for ciliogenesis and Hedgehog signalling across the vertebrates. Development *138*, 4969–4978.
18. Davey, M.G., Paton, I.R., Yin, Y., Schmidt, M., Bangs, F.K., Morrice, D.R., Smith, T.G., Buxton, P., Stamataki, D., Tanaka, M., et al. (2006). The chicken talpid3 gene encodes a novel protein essential for Hedgehog signaling. Genes Dev. *20*, 1365–1377.
19. Bachmann-Gagescu, R., Phelps, I.G., Dempsey, J.C., Sharma, V.A., Ishak, G.E., Boyle, E.A., Wilson, M., Marques Lourenço, C., and Arslan, M.; University of Washington Center for Mendelian Genomics (2015). KIAA0586 is Mutated in Joubert Syndrome. Hum. Mutat. *36*, 831–835.

20. Malicdan, M.C.V., Vilboux, T., Stephen, J., Maglic, D., Mian, L., Konzman, D., Guo, J., Yildirimli, D., Bryant, J., Fischer, R., et al. (2015). Mutations in human homologue of chicken talpid3 gene (KIAA0586) cause a hybrid ciliopathy with overlapping features of Jeune and Joubert syndromes. J. Med. Genet. *52*, 830–839.

21. Stephen, L.A., Tawamie, H., Davis, G.M., Tebbe, L., Nürnberg, P., Nürnberg, G., Thiele, H., Thoenes, M., Boltshauser, E., Uebe, S., et al. (2015). TALPID3 controls centrosome and cell polarity and the human ortholog KIAA0586 is mutated in Joubert syndrome (JBTS23). Elife *4*, e08077.

22. Lim, L.P., and Burge, C.B. (2001). A computational analysis of sequence features involved in recognition of short introns. Proc. Natl. Acad. Sci. USA *98*, 11193–11198.

23. Wallmeier, J., Nielsen, K.G., Kuehni, C.E., Lucas, J.S., Leigh, M.W., Zariwala, M.A., and Omran, H. (2020). Motile ciliopathies. Nat. Rev. Dis. Prim. *6*, 77.

24. Stenram, U., Cramnert, C., and Axfors-Olsson, H. (2007). Oralfacialdigital-like syndrome with respiratory tract symptoms from birth and ultrastructural centriole/basal body disarray. Acta Paediatr. *96*, 1101–1104.

25. Forsythe, E., and Beales, P.L. (2013). Bardet-Biedl syndrome. Eur. J. Hum. Genet. *21*, 8–13.

26. Waters, A.M., and Beales, P.L. (2011). Ciliopathies: an expanding disease spectrum. Pediatr. Nephrol. *26*, 1039–1056.

27. Gerdes, J.M., Davis, E.E., and Katsanis, N. (2009). The vertebrate primary cilium in development, homeostasis, and disease. Cell *137*, 32–45.

28. Mitchison, H.M., and Valente, E.M. (2017). Motile and non-motile cilia in human pathology: from function to phenotypes. J. Pathol. *241*, 294–309.

29. Praveen, K., Davis, E.E., and Katsanis, N. (2015). Unique among ciliopathies: primary ciliary dyskinesia, a motile cilia disorder. F1000Prime Rep. *7*, 36.

30. Stephen, L.A., Davis, G.M., McTeir, K.E., James, J., McTeir, L., Kierans, M., Bain, A., and Davey, M.G. (2013). Failure of centrosome migration causes a loss of motile cilia in talpid(3) mutants. Dev. Dynam. *242*, 923–931.

31. Wu, C., Yang, M., Li, J., Wang, C., Cao, T., Tao, K., and Wang, B. (2014). Talpid3-binding centrosomal protein Cep120 is required for centriole duplication and proliferation of cerebellar granule neuron progenitors. PLoS One *9*, e107943.

32. Kobayashi, T., Kim, S., Lin, Y.-C., Inoue, T., and Dynlacht, B.D. (2014). The CP110-interacting proteins Talpid3 and Cep290 play overlapping and distinct roles in cilia assembly. J. Cell Biol. *204*, 215–229.

33. Wang, L., Lee, K., Malonis, R., Sanchez, I., and Dynlacht, B.D. (2016). Tethering of an E3 ligase by PCM1 regulates the abundance of centrosomal KIAA0586/Talpid3 and promotes ciliogenesis. Elife *5*, e12950.

34. Wang, L., Failler, M., Fu, W., and Dynlacht, B.D. (2018). A distal centriolar protein network controls organelle maturation and asymmetry. Nat. Commun. *9*, 3938.

35. Ojeda Naharros, I., Cristian, F.B., Zang, J., Gesemann, M., Ingham, P.W., Neuhauss, S.C.F., and Bachmann-Gagescu, R. (2018). The ciliopathy protein TALPID3/KIAA0586 acts upstream of Rab8 activation in zebrafish photoreceptor outer segment formation and maintenance. Sci. Rep. *8*, 2211.

36. Tsai, J.J., Hsu, W.B., Liu, J.H., Chang, C.W., and Tang, T.K. (2019). CEP120 interacts with C2CD3 and Talpid3 and is required for centriole appendage assembly and ciliogenesis. Sci. Rep. *9*, 6037.

37. Wang, J., Li, T., Wang, J.L., Xu, Z., Meng, W., and Wu, Q.F. (2020). Talpid3-Mediated Centrosome Integrity Restrains Neural Progenitor Delamination to Sustain Neurogenesis by Stabilizing Adherens Junctions. Cell Rep. *33*, 108495.

38. Yan, H., Chen, C., Chen, H., Hong, H., Huang, Y., Ling, K., Hu, J., and Wei, Q. (2020). TALPID3 and ANKRD26 selectively orchestrate FBF1 localization and cilia gating. Nat. Commun. *11*, 2196.

39. Frase, A.M. (2019). DaveyMG TALPID3 in Joubert syndrome and related ciliopathy disorders. Curr. Opin. Genet. Dev. *6*, 41–48.

40. Cruz, C., Ribes, V., Kutejova, E., Cayuso, J., Lawson, V., Norris, D., Stevens, J., Davey, M., Blight, K., Bangs, F., et al. (2010). Foxj1 regulates floor plate cilia architecture and modifies the response of cells to sonic hedgehog signalling. Development *137*, 4271–4282.

41. Dodd, D.O., Mechaussier, S., Yeyati, P.L., McPhie, F., Anderson, J.R., Khoo, C.J., Shoemark, A., Gupta, D.K., Attard, T., Zariwala, M.A., et al. (2024). Ciliopathy patient variants reveal organelle-specific functions for TUBB4B in axonemal microtubules. Science *384*, eadf5489.

42. Lee, Y.L., Santé, J., Comerci, C.J., Cyge, B., Menezes, L.F., Li, F.Q., Germino, G.G., Moerner, W.E., Takemaru, K.I., and Stearns, T. (2014). Cby1 promotes Ahi1 recruitment to a ring-shaped domain at the centriole-cilium interface and facilitates proper cilium formation and function. Mol. Biol. Cell *25*, 2919–2933.

43. Bukowy-Bieryllo, Z., Rabiasz, A., Dabrowski, M., Pogorzelski, A., Wojda, A., Dmenska, H., Grzela, K., Sroczynski, J., Witt, M., and Zietkiewicz, E. (2019). Truncating mutations in exons 20 and 21 of OFD1 can cause primary ciliary dyskinesia without associated syndromic symptoms. J. Med. Genet. *56*, 769–777.

44. Dulla, K., Aguila, M., Lane, A., Jovanovic, K., Parfitt, D.A., Schulkens, I., Chan, H.L., Schmidt, I., Beumer, W., Vorthoren, L., et al. (2018). Splice-Modulating Oligonucleotide QR-110 Restores CEP290 mRNA and Function in Human c.2991+1655AG LCA10 Models. Mol. Ther. Nucleic Acids *12*, 730–740.

45. Tomkiewicz, T.Z., Suárez-Herrera, N., Cremers, F.P.M., Collin, R.W.J., and Garanto, A. (2021). Antisense Oligonucleotide-Based Rescue of Aberrant Splicing Defects Caused by 15 Pathogenic Variants in ABCA4. Int. J. Mol. Sci. *22*, 4621.

46. Vaz-Drago, R., Custódio, N., and Carmo-Fonseca, M. (2017). Deep intronic mutations and human disease. Hum. Genet. *136*, 1093–1111.

47. González-Del Pozo, M., Martín-Sánchez, M., Bravo-Gil, N., Méndez-Vidal, C., Chimenea, Á., Rodríguez-de la Rúa, E., Borrego, S., and Antiñolo, G. (2018). Searching the second hit in patients with inherited retinal dystrophies and monoallelic variants in ABCA4, USH2A and CEP290 by whole-gene targeted sequencing. Sci. Rep. *8*, 13312.

48. Romano, M., Buratti, E., and Baralle, D. (2013). Role of pseudoexons and pseudointrons in human cancer. Int. J. Cell Biol. *2013*, 810572.

49. Dhir, A., and Buratti, E. (2010). Alternative splicing: role of pseudoexons in human disease and potential therapeutic strategies. FEBS J. *277*, 841–855.

50. Keegan, N.P., Wilton, S.D., and Fletcher, S. (2021). Analysis of Pathogenic Pseudoexons Reveals Novel Mechanisms Driving Cryptic Splicing. Front. Genet. *12*, 806946.

51. Roosing, S., Hofree, M., Kim, S., Scott, E., Copeland, B., Romani, M., Silhavy, J.L., Rosti, R.O., Schroth, J., Mazza, T., et al. (2015). Functional genome-wide siRNA screen identifies KIAA0586 as mutated in Joubert syndrome. Elife *4*, e06602.

52. Olbrich, H., Horváth, J., Fekete, A., Loges, N.T., Storm van's Gravesande, K., Blum, A., Hörmann, K., and Omran, H. (2006). Axonemal localization of the dynein component DNAH5 is not altered in secondary ciliary dyskinesia. Pediatr. Res. *59*, 418–422.

53. Hirst, R.A., Rutman, A., Williams, G., and O'Callaghan, C. (2010). Ciliated air-liquid cultures as an aid to diagnostic testing of primary ciliary dyskinesia. Chest *138*, 1441–1447.

54. Munye, M.M., Shoemark, A., Hirst, R.A., Delhove, J.M., Sharp, T.V., McKay, T.R., O'Callaghan, C., Baines, D.L., Howe, S.J., and Hart, S.L. (2017). BMI-1 extends proliferative potential of human bronchial epithelial cells while retaining their mucociliary differentiation capacity. Am. J. Physiol. Lung Cell Mol. Physiol. *312*, L258–L267.

55. Glaus, E., Schmid, F., Da Costa, R., Berger, W., and Neidhardt, J. (2011). Gene therapeutic approach using mutation-adapted U1 snRNA to correct a RPGR splice defect in patient-derived cells. Mol. Ther. *19*, 936–941.

56. Song, F., Owczarek-Lipska, M., Ahmels, T., Book, M., Aisenbrey, S., Menghini, M., Barthelmes, D., Schrader, S., Spital, G., and Neidhardt, J. (2021). High-Throughput Sequencing to Identify Mutations Associated with Retinal Dystrophies. Genes *12*, 1269.

57. Altmüller, J., Motameny, S., Becker, C., Thiele, H., Chatterjee, S., Wollnik, B., and Nürnberg, P. (2016). A systematic comparison of two new releases of exome sequencing products: the aim of use determines the choice of product. Biol. Chem. *397*, 791–801.

58. Raidt, J., Wallmeier, J., Hjeij, R., Onnebrink, J.G., Pennekamp, P., Loges, N.T., Olbrich, H., Häffner, K., Dougherty, G.W., Omran, H., and Werner, C. (2014). Ciliary beat pattern and frequency in genetic variants of primary ciliary dyskinesia. Eur. Respir. J. *44*, 1579–1588.

59. Davison, A.C., and Hinkley, D.V. (1997). Bootstrap Methods and Their Application (Cambridge Univ. Press).

60. Da Costa, R., Glaus, E., Tiwari, A., Kloeckener-Gruissem, B., Berger, W., and Neidhardt, J. (2015). Localizing the RPGR protein along the cilium: a new method to determine efficacies to treat RPGR mutations. Gene Ther. *22*, 413–420.

STAR★METHODS

KEY RESOURCES TABLE

REAGENT or RESOURCE	SOURCE	IDENTIFIER
Antibodies		
Mouse monoclonal anti-acetylated alpha tubulin (clone 6-11B-1)	Sigma Aldrich	Cat#T6793; RRID: AB_477585
Mouse monoclonal anti-γ-tubulin	Abcam	Cat#ab11316; RRID: AB_297920
Rabbit polyclonal anti-detyrosinated tubulin	Merck	Cat#AB3201; RRID: AB_177350
Rabbit polyclonal anti-CEP164	Origene	Cat#AP50843PU-N; RRID: AB_11148126
Donkey anti-mouse IgG conjugated with Alexa Fluor 488	Life Technologies	Cat#A21202; RRID: AB_141607
Donkey anti-rabbit IgG conjugated with Alexa Fluor 568	Life Technologies	Cat#A10042; RRID: AB_2534017
Donkey anti-rabbit IgG conjugated with Alexa Fluor 647	Life Technologies	Cat#A31573; RRID: AB_2536183
Goat anti-mouse IgG conjugated with Alexa Fluor 488	Invitrogen	Cat#A11029; RRID: AB_2534088
Goat anti-rabbit IgG conjugated with Alexa Fluor 546	Invitrogen	Cat#A11035; RRID: AB_2534093
Hoechst 33342	Sigma Aldrich	Cat#14533; RRID: AB_2651135
Biological samples		
Patient- and unrelated control-derived respiratory epithelial cells	this study	N/A
Patient- and unrelated control-derived primary fibroblasts	this study	N/A
Chemicals, peptides, and recombinant proteins		
DAKO fluorescence Mounting medium	Dako North America	Cat#S3023
Gibco™ DMEM-Ham's F12	Thermo Fisher	Cat#11039.012
Exo-SAP	New England Biolabs	Cat#M0293S, Cat#M0371S
Gibco™ fetal bovine serum	Invitrogen	Cat#10270-1056
Fluoromount-G	SouthernBiotech	Cat#0100-20
Gibco™ Antibiotic-Antimycotic	Thermo Fisher	Cat#15240062
Gibco™ RPMI medium	Thermo Fisher	Cat#21875-034
GoTaq G2 Flexi DNA Polymerase	Promega	Cat#M7805
HotFirePol DNA Polymerase	Solis BioDyne	Cat#01-02-00500
L-glutamine	Biowest	Cat#X0550
Minimum Essential Medium	Biowest	Cat#L0440-500
NU serum	Becton Dickinson	Cat#355504
Penicillin-Streptomycin solution	Biowest	Cat#L0022
PneumaCult™-ALI Medium	Stemcell™	Cat#05001
Shandon Cryomatrix Frozen Embedding Medium	Thermo Scientific	Cat#6769006
SuperScript III	Invitrogen	Cat#18080093
Critical commercial assays		
BigDye® Terminator v3.1 Cycle Sequencing Kit	Applied Biosystems™	Cat#4337457
Gentra Puregene kit	QIAGEN	Cat#158467C
Nucleospin RNA Isolation Kit	Macherey & Nagel	Cat#740955.50
Oligonucleotides		
KIAA0586_ex26-28_F: agtcagcagtttcccagcaa	Metabion	N/A
KIAA0586_ex26-28_R: gctgtcagaagtgttgtggg	Metabion	N/A
random primer	Metabion	N/A
KIAA0586_ex14-16_F: tatcagggccatcgaagcac	Metabion	N/A
KIAA0586_ex14-16_R: ttacagggtgtggcttgctg	Metabion	N/A
KIAA0586_ex15-17_F: ggtcatctgattcctatggcaa	Metabion	N/A

(*Continued on next page*)

Continued

REAGENT or RESOURCE	SOURCE	IDENTIFIER
KIAA0586_ex15-17_R: tgcacaggaggaagagatgc	Metabion	N/A
KIAA0586_ex17-20_F: acccagtgtagatattgacagca	Metabion	N/A
KIAA0586_ex17-20_R: ttgctggactggaaagagcc	Metabion	N/A
KIAA0586_ex22-24_F: gctcaccttcatcacctgct	Metabion	N/A
KIAA0586_ex22-24_R: gaggctgagcagggaaatcc	Metabion	N/A
KIAA0586_ex24-26_f: cctcacagatgccaggttct	Metabion	N/A
KIAA0586_ex24-26_R: ctgaatgatagactgcttgctgg	Metabion	N/A
Software and algorithms		
Adobe Creative Suites CS5	–	RRID:SCR_010279
Amira software	Thermo Fisher Scientific	https://www.thermofisher.com/order/catalog/product/de/de/AMIRA
CodonCode Aligner (v.3.7.1)	CodonCode Corporation	https://www.codoncode.com/productsservices/aligner.htm
Fiji-ImageJ	https://imagej.nih.gov/ij/	RRID: SCR_003070
GraphPad Prism (version 9.5.1)	GraphPad Software, LLC	RRID: SCR_002798 https://www.graphpad.com
GraphPad PRISM9 (2020)	GraphPad Software, LLC	RRID: SCR_002798 https://www.graphpad.com
IBM SPSS Statistics (version 27)	IBM	RRID:SCR_016479
IMOD	University of Colorado Boulder	RRID:SCR_003297
LAS-X	Leica	RRID:SCR_013673
Nis-Elements Advanced Research	Nikon	RRID:SCR_014329
R	–	RRID:SCR_001905
Sisson-Ammons Video Analysis (SAVA) System	Ammons Engineering	https://www.ammonsengineering.com/SAVA.html
SnapGene software	GLS Biotech	RRID:SCR_015052
ZEN-blue and ZEN-black software	Zeiss	RRID:SCR_013672
Other		
Costar Corning Transwell clear polyester membrane inserts	Corning Inc.	Cat#3470
SuperFrost Plus microscope slides	Thermo Scientific	Cat#J1800AMNZ

EXPERIMENTAL MODEL AND STUDY PARTICIPANT DETAILS

Ethics statement

All experiments were carried out in accordance to the principles of the World Medical Association Declaration of Helsinki. Signed informed consent was obtained from all individuals (affected patients and relatives) included in the study, based on protocols approved by the local ethics committee of the Medizinische Hochschule Hannover (Nr.2576-2015), the University of Oldenburg (2018-097), the University of Münster, and cooperating institutions. Human cells were analyzed from family 1 (II.I male, German; II.II female, German), family 2 (II.I female, Sweden) and family 3 (II.I male, German).

Culture of respiratory epithelial cells

Nasal brush biopsies were performed to obtain respiratory epithelial cells of the middle turbinate from the affected individuals. Nasal brushes (Engelbrecht Medicine and Laboratory technology) were subsequently rinsed in Gibco™ RPMI medium supplemented with Gibco™ Antibiotic-Antimycotic (Thermo Fisher). The cell suspension was proceeded for cell culture. First, respiratory cells were pre-cultured in rat-collagen coated cell culture flasks to increase cell number before proceeded to spheroid cells using Gibco™ DMEM-Ham's F12 (Thermo Fisher) supplemented with 10% NU serum (Becton Dickinson) or for ALI-cultures as already described.[52–54] For ALI cultures, basal cells were seeded onto the rat-collagen coated membranes of Transwell inserts (Costar Corning 3470 Transwell clear polyester membrane inserts; Corning Inc.) that fit into 24 well plates. During the proliferation phase cells were fed from the basal and apical compartment with PneumaCult™-Ex Medium (Stemcell™). To initiate differentiation (airlift), PneumaCult™-ALI Medium (Stemcell™) was given to the basal compartment only while the apical cell layer had direct air contact. After 30 days post airlift cells were fully differentiated and used for follow-up techniques such as TEM, IF staining and high-speed video microscopy. ALI-cultured

cells originated from II.I (male) of family 1, respiratory epithelial cells were derived from II.II (female) of family 1, and spheroid cell culture was performed from II.I (male) of family 3.

Culture of fibroblast cells

Patient- and unrelated control-derived (male) primary fibroblasts were obtained from a skin biopsy as previously described.[55] Briefly, the skin biopsy was cut into small fragments and transferred to a sterile culture flask. After adherence of the tissue fragments, culture medium (Minimum Essential Medium (MEM; L0440-500, Biowest) with 20% fetal bovine serum (Biowest), 1.3%-L-glutamine (Biowest) and 0.8% antibiotic-antimyotic solution (Biowest)) was added. The cultures were maintained at 37°C in a 5% CO2 incubator for 5-10 days. Once fibroblasts had grown sufficiently, they were harvested and transferred to a 75 cm^2 flask for further expansion. Human dermal fibroblasts were cultured at 37°C and 5% CO_2 in MEM (L0440-500, Biowest) supplemented with 20% fetal bovine serum (Biowest), 1.4%-L-glutamine (Biowest) and 1% Penicillin-Streptomycin solution (Biowest). Fibroblast cells were tested for mycoplasma contamination by PCR. Fibroblasts were cultured from patient II.I (male) and II.II (female) of family 1.

METHOD DETAILS

DNA extraction and genetic analysis

EDTA blood samples of available family members or cell pellets from patient-derived fibroblasts were used for molecular genetic analyses. DNA samples were prepared according to manufacturer's instructions using the Gentra Puregene kit (QIAGEN). Quantity and quality of DNA samples were analysed using UV spectrometry (Biospectrometer). For patients of family 1 and 2 WES was performed as described by Song *et al.*[56] For patient (II.I) of family 3, WES was applied as described by Altmüller *et al.*[57] A total of 124 JS patients, predominantly originating from Italy and The Netherlands, were screened for the variant *KIAA0586/TALPID3*:c.[3990+3186G>A] (NM_001329943.3) using Sanger sequencing.

PCR amplification and sanger sequencing

Forward and reverse primers located in regions of interest of the human *KIAA0586/TALPID3* were designed using Primer Input3 (https://primer3.ut.ee). Additionally, the primer binding sites in the human genome (GRCh37/hg19) were verified for known single-nucleotide polymorphisms (SNPs) using SNPCheck (https://secure.ngrl.org.uk/SNPCheck/). PCR amplification of target regions was performed with 10-20 ng of genomic DNA using HotFirePol DNA Polymerase (Solis BioDyne) or GoTaq G2 Flexi DNA Polymerase (Promega) according to standard protocols. For Sanger sequencing, the PCR amplicons were enzymatically purified with ExoSAP (New England Biolabs (NEB), Frankfurt, Germany) and sequenced using BigDye® Terminator v3.1 Cycle Sequencing Kit on 3730xl DNA Analyzer or ABI Prism 3130xl Genetic Analyzer (Applied Biosystem). Sequencing data were analysed using the SnapGene software (GLS Biotech) or CodonCode Aligner (v.3.7.1).

TEM and 3D tomography

Respiratory epithelial cells cultured as spheroids or under ALI-conditions were fixed in 2.5% glutaraldehyde overnight at 4°C. 1% osmium tetroxide was used to stain the sample material. Using 1,2-epoxypropan-epon mixture in a ratio of 1:1 the samples incubated overnight at 4 °C for full permeabilization. Epon-embedded samples were sectioned before transfer onto copper grids. Sections were contrasted with uranyl acetate and For 3D tomography sections were briefly incubated with 10 nm colloidal gold particles before imaging. A single-tilt series was collected manually from -40° to 40° with 5° intervals and a final pixel size of 1·458 nm. The corresponding 3D tomogram was aligned and reconstructed using IMOD software, rendering was done with Amira software (Thermo Fisher Scientific).

IF staining of respiratory epithelial cells

Respiratory epithelial cells were used for IF staining. Fully differentiated ALI-cultures were first embedded in Tissue-Tek Cryomolds (Sakura) with Thermo Scientific Shandon Cryomatrix Frozen Embedding Medium. Sectioned into 20 μm longitudinal sections using the Leica CM3050S Cryostat, sample material was transferred to Thermo Scientific SuperFrost Plus microscope slides.

IF staining was performed as reported by Wallmeier *et al.*[15] In brief, cells were fixed with 4% paraformaldehyde (PFA), permeabilized with 0.2%Triton-X (diluted in Dulbecco's phosphate-buffered saline (PBS; GibcoTM)) before blocked with 2% bovine serum albumin (BSA; w/v)/5% goat serum (v/v diluted in PBS) or 1% skim milk (w/v diluted in PBS). Diluted in blocking solution, the following primary (i) and secondary (ii) antibodies were used: (i) mouse monoclonal anti-acetylated alpha tubulin clone 6-11B-1 (T6793; Sigma Aldrich; 1:10,000) and rabbit polyclonal anti-CEP164 (AP50843PU-N; Origene; 1:100) incubated 4 h at room temperature or overnight at 4°C as well as (ii) goat anti-mouse IgG conjugated with Alexa Fluor 488 (A11029; Invitrogen; 1:1,000) and goat anti-rabbit IgG conjugated with Alexa Fluor 546 (A11035; Invitrogen; 1:1,000) incubated 30-60 minutes at room temperature. Nuclei were stained with Hoechst 33342 (14533-100MG, Sigma-Aldrich) diluted 1:1,000 in PBS. Slides were finally mounted with DAKO fluorescent Mounting medium (Dako North America). Images were taken with the Leica THUNDER Imager System and LAS-X software program or the Zeiss Apotome Axiovert 200 microscope and ZEN-blue and ZEN-black software programs. For final image processing the Adobe Creative Suites CS5 were used.

High-speed video microscopy

Cultured as spheroids or under ALI-conditions, ciliary beating was analysed by high-speed video microscopy using a Basler acA1300-200um monochrome high-speed video camera attached to the inverted phase-contrast Zeiss Axio Vert A1 microscope as described by Raidt *et al.*[58] In addition, the Leica THUNDER Imager System and the software program LAS-X were used. Videos were taken at 37°C with a 40x objective lens. To determine the CBF (in Hz) as well as the active area (in %) the whole-field analysis approach was performed using the Sisson-Ammons Video Analysis (SAVA) System (Ammons Engineering, Mt. Morris, USA). For statistical evaluation, the software program GraphPad Prism Version 9.5.1 was used.

Particle tracking experiments

Particle Tracking experiments were performed with fully differentiated ALI-cultures as described detailly by Wallmeier *et al.*[14,23] In brief, cells were washed with PBS two times before 100 μl pre-warmed PneumaCult™-ALI Medium was added to the apical compartment to determine the ciliary beat frequency as well as active area as described above. Afterwards, additional 100 μl pre-warmed PneumaCult™-ALI Medium was added to the apical compartment including 2 μm-sized fluorescent beads. Particle tracking videos each consisting of 150 single pictures separated by 550 ms were taken with the Leica THUNDER Imager System equipped with a 10x objective lens. The software program LAS-X and NIS-Elements Advanced Research software was used to extract AVI videos, which were analysed employing the NIS-Elements Advanced Research software to yield position and timing information of all detected fluorescent beads. Data derived from positions with greater distance than 2.5 mm to the center of the insert were removed to avoid border effects from the boundary of the insert at a radius of 3 mm. Yielding a representative velocity value for each insert, the data have been thoroughly analysed. Local velocity differences and imbalanced fluorescent beads distribution were thoroughly averaged by the following procedure. For each identified fluorescent bead a velocity value is assigned for each of two consecutive pictures. All velocity values were sorted in a regularly spaced 5x5 grid. For each cell of the grid a mean value has been calculated. The 95% confidence interval has been derived by a bootstrapping approach.[59] The equally weighted mean of the 25 cells yield the velocity value of the insert. The 95% confidence interval has been derived by the same bootstrapping approach as described above. For statistical evaluation, three ALI-Inserts per individual were analysed in total (seven positions tracked three times resulting in 21 videos per Insert in total) using a customized R-script and GraphPad Prism Version 9.5.1. Z-Stack projections were created with FIJI.

RNA isolation and RT-PCR analyses

After 48 h incubation, fibroblasts were washed with ice cold PBS and lysed with 350 μl of lysis buffer RA1 (Macherey & Nagel) containing 3·5 μl β-mercaptoethanol (Serva). Lysates were harvested by scraping with a pipette tip in combination with pipetting up and down at least three times. The total RNA was purified according to the manufacturer's manual (Nucleospin RNA Isolation Kit, Macherey & Nagel). First-strand cDNA was generated using 500 ng of RNA with random primers (Metabion) and reverse transcriptase (SuperScript III, Invitrogen). Reverse transcription was performed according to standard protocols. To amplify the transcript of interest, 1 μl of cDNA was used. Amplification was performed using HotFire Taq Polymerase (Solis Biodyne) according to manufacturer's recommendations. PCR products were analysed by agarose gel electrophoresis (1 to 1.5% agarose gels in TAE buffer). Primer sequences are available in the key resource table.

Immunocytochemistry of fibroblast cells

For analysis fibroblast were seeded in twelve-well plates on coverslips (12 mm) in supplemented MEM and incubated for 24 h at 37 °C and 5% CO_2, followed by nutrition deprivation for 48 h at 37 °C, 5% CO_2 in MEM without FBS, but containing 1.25% Penicillin-Streptomycin solution and 1.75% L-glutamine. After 48 h incubation, cells were fixed with 4% PFA (Carl Roth) and blocked in PBS containing 2.5% BSA (fraction V, Carl Roth) and 0.1% Tween-20 (AppliChem). Immunocytochemistry staining was performed with primary antibodies raised against detyrosinated tubulin (AB3201; Merck; 1:1000; rabbit polyclonal) and γ-tubulin (ab11316; Abcam; 1:500; mouse monoclonal). Donkey anti-mouse IgG conjugated with Alexa Fluor 488 (A21202; Life Technologies; 1:2000) and donkey anti-rabbit IgG conjugated with Alexa Fluor 568/647 (A10042/A31573; Life Technologies; 1:1000) were used as secondary antibodies. Coverslips were mounted with mounting medium containing 4′,6-Diamidin-2-phenylindol (DAPI) (Fluoromount-G, SouthernBiotech). Slides were analysed with a Zeiss Axio Observer 7 microscope (Carl Zeiss) using a 40×/0.6 Corr Ph2 M27 plan apochromat objective. All images were taken with the same illumination intensity and exposure time. Image processing was conducted using ZEN 3.4 (blue edition) software (Zeiss) and Fiji-ImageJ (ImageJ 1.53c; https://fiji.sc/).

Measurements of primary cilia

To analyse the length of the primary cilia, 250 cilia per cell line were measured in three independent experiments (in total 750 cilia per cell line) as previously described.[60] For each experiment, cells were seeded independently on different days at different passage numbers (between 6 and 12). The length of the axoneme of the primary cilia was determined using Fiji-ImageJ (segmented line tool). Statistical analysis was performed using IBM SPSS Statistics software (version 27) and GraphPad PRISM9 (2020). Statistical significance was analysed using the non-parametric Kruskal-Wallis test. A p-value of <0.05 was regarded statistically significant.

QUANTIFICATION AND STATISTICAL ANALYSIS

For Statistical analysis IBM SPSS Statistics software (version 27) and GraphPad PRISM9 (2020)/GraphPad Prism Version 9.5.1 was used. Statistical significance was analysed using the non-parametric Kruskal-Wallis test followed by multiple pairwise-comparisons to assess differences in the length of primary cilia in patient-derived fibroblasts compared to unrelated controls. Results were considered statistically significant based on a p-value less than 0.05. The details can be found in the figure legends and method details.